Chinese Chemical Letters 37 (2026) 111445

Contents lists available at ScienceDirect

Chinese Chemical Letters

journal homepage: www.elsevier.com/locate/cclet

Enhanced anodic mass transfer enables interfacial Cl• for efficient ammonia oxidation

Xia Chen[a], Ting Dai[a], Meng-Ying Yin[a], Xing-Yuan Xia[a], Qiu-Ju Xing[a], Lei Tian[a,b,*], Jian-Ping Zou[a,*]

[a] Key Laboratory of Jiangxi Province for Persistent Pollutants Prevention Control and Resource Reuse, Nanchang Hangkong University, Nanchang 330063, China

[b] School of Chemistry and Chemical Engineering, Institute of Clean Energy and Materials, Key Laboratory for Clean Energy and Materials, Ministry of Education, Guangzhou University, Guangzhou Higher Education Mega Center, Guangzhou 510006, China

ARTICLE INFO

Article history:
Received 20 December 2024
Revised 22 April 2025
Accepted 10 June 2025
Available online 11 June 2025

Keywords:
Electrocatalytic system
Ammonia-nitrogen oxidation
Chlorine radical
Mass transfer
Mineralization

ABSTRACT

The electrostatic repulsion between the anode and ammonia (NH_4^+) can cause chlorine radicals ($Cl^•$) at the interface to self-compounding into low oxidating species, weakening the treatment performance of ammonia-nitrogen (NH_4^+-N) wastewater. This study introduces electron-rich elements into the tetrahedral sites (A_{Td}^{2+}) of spinel cobalt oxide (Co_3O_4) for efficient and selective NH_4^+-N mineralization induced by interfacial $Cl^•$. Batch experiments, *in-situ* characterizations, and theoretical calculations confirm that Cu_{Td}^{2+} have moderate energy level matching and strong binding energy with NH_4^+ compared to Ni_{Td}^{2+} and Zn_{Td}^{2+}. NH_4^+ can effectively overcome electrostatic repulsion and enrich on $Cu_xCo_{3-x}O_4$ anode. More importantly, the interaction of Cu_{Td}^{2+}-O-Co_{Oh}^{3+} weakens the binding of $Cl^•$ at Co_{Oh}^{3+} sites, promoting the desorption of $Cl^•$ from the anodic interface. As a result, NH_4^+-N is mineralized by $Cl^•$ into N_2 with a rate of 4.4×10^{-2} min^{-1}, superior to Co_3O_4 and commercial dimensionally stable anodes. Finally, the scale-up experiment using a continuous flow reactor realizes long-term stability for NH_4^+-N wastewater treatment, in which 100 % of NH_4^+-N and 88.3 % of total nitrogen can be continuously eliminated in 96 h. This study offers an in-depth understanding of interfacial reactions in the EC system and guides the design and synthesis of superior anodes for environmental remediation.

© 2025 Published by Elsevier B.V. on behalf of Chinese Chemical Society and Institute of Materia Medica, Chinese Academy of Medical Sciences.

The rapid development of industrialization and urbanization has caused abundant amounts of ammonia (NH_4^+/NH_3) in wastewater [1,2]. The discharge of ammonia nitrogen into natural water bodies can result in severe water contamination and accelerate the process of eutrophication, which has serious harm to the ecological environment [3]. Therefore, it is urgent to develop a green and efficient technology for the treatment of ammonia nitrogen in wastewater in light of the call for energy conservation and emission reduction [4–6].

Many efforts have been made to treat ammonia nitrogen by various technologies including air stripping [7,8], biological denitrification [9,10], and breakpoint chlorination [11,12]. Nevertheless, these methods have inherent limitations [13,14]. For instance, the air stripping exhibits poor removal efficiency for ammonia nitrogen with low concentration. Biological denitrification is easily disturbed by temperature and C/N ratio of wastewater and a long treatment period is required. Breakpoint chlorination is commonly observed in the chlorination of ammonia-containing wastewater treatments but its high cost and complex operation remain a problem. Recently, the electrocatalytic (EC) system based on the anodic chlorine evolution reaction (CER) has been identified as a highly sustainable approach for ammonia nitrogen removal due to its superior oxidation capacity / easy operation / regulation [15–17]. A wide variety of chlorine-containing active species can be produced in the EC system, which can efficiently and selectively oxidize ammonia into nitrogen (N_2) [18,19]. Among these chlorine-containing active species, chlorine radical ($Cl^•$) has a higher redox potential (2.55 V *vs.* SHE) than HClO/ClO^- (1.49/0.89 V *vs.* SHE), $ClO^•$ (1.39 V *vs.* SHE), and $Cl_2^{•-}$ (2.13 V *vs.* SHE) [20,21], thereby conferring a significant advantage in the removal of ammonia. Designed to produce $Cl^•$ for water purification, a lot of advanced systems are developed, such as the photoelectrocatalytic system [22,23] and the EC system coupled with the advanced oxidation process [24]. However, due to the high reaction activity with Cl^- (8.00×10^9 L mol^{-1} s^{-1}), HClO/ClO^- ($3.00/8.30 \times 10^9$ L mol^{-1} s^{-1}), and OH^- (1.80×10^{10} L mol^{-1} s^{-1}), $Cl^•$ is easily quenched into low re-

* Corresponding authors.
E-mail addresses: leitian3315@126.com (L. Tian), zjp_112@126.com (J.-P. Zou).

https://doi.org/10.1016/j.cclet.2025.111445
1001-8417/© 2025 Published by Elsevier B.V. on behalf of Chinese Chemical Society and Institute of Materia Medica, Chinese Academy of Medical Sciences.

active species [13,25]. The difficulty of controllable generation of Cl• in catalytic systems for ammonia removal is extremely high. Therefore, it is urgent to develop novel systems to efficiently and controllably produce Cl• for the treatment of ammonia nitrogen wastewater.

Volmer step: $Cl^-_{(aq)} \rightarrow Cl^* + e^-$ (1)

Heyrovsky step: $Cl^* + Cl^-_{(aq)} \rightarrow Cl_{2(g)} + e^-$ (2)

Tafel step: $Cl^* + Cl^* \rightarrow Cl_{2(g)}$ (3)

It is found from the Volmer step in CER that Cl^- can be oxidized into adsorbed Cl• (Cl*) (Eq. 1) [26]. The adsorbed Cl• will undergo self-quenching into chlorine gas (Cl_2) (Eqs. 2 and 3) [27,28]. If the adsorbed Cl• at the anode interface can react with ammonia nitrogen and suppress their self-quenching, the Cl•-mediated ammonia nitrogen mineralization process can be effectively and selectively achieved. However, in the CER-mediated ammonia nitrogen oxidation system, the active sites of the anode usually have a strong binding energy with Cl^- [16,29,30], which suppresses the adsorbed Cl• overflowing from the interface for ammonia nitrogen oxidation. More seriously, the pH of ammonia nitrogen wastewater is generally neutral or weakly acidic, and ammonia mainly exists in the form of NH_4^+ ($pK_a(NH_4^+/NH_3) = 9.25$) [31]. There is a strong electrostatic repulsion between NH_4^+ and the anode, which prevents the enrichment of NH_4^+ on the anodic interface to react with Cl•. These results make it difficult for Cl• in the CER process to efficiently remove ammonia nitrogen, seriously affecting the treatment efficiency of ammonia nitrogen wastewater. Spinel oxides (AB_2O_4) with excellent electrochemical activity and adjustable electronic structure are the potential anode materials for the Cl•-mediated ammonia nitrogen oxidation process [32–34]. In detail, the octahedral sites (B_{Oh}^{3+}) with a high oxidation potential can effectively oxidize Cl^- to Cl•, while the tetrahedral sites (A_{Td}^{2+}) with a high energy level matching with NH_4^+ may effectively enrich NH_4^+. Modulating the elements of A_{Td}^{2+} can not only enhance the binding energy with NH_4^+ but also promote Cl• overflow from B_{Oh}^{3+}. Therefore, the design and development of the novel AB_2O_4 anode to efficiently rich NH_4^+ and produce Cl• is of great significance for the removal of ammonia nitrogen wastewater.

Hence, this study introduces other ions such as Ni^{2+}, Cu^{2+}, or Zn^{2+} into the A_{Td}^{2+} of Co_3O_4 to induce the efficient enrichment of NH_4^+ and the production of Cl• at the anode, which realizes the Cl•-mediated ammonia nitrogen oxidation process (Fig. 1a). Due to the high redox potential ($E^0 = 1.81$ V) and rapid Co^{2+}/Co^{3+} cycle, Cl^- can be efficiently oxidized into Cl• at Co_{Oh}^{3+} [35,36]. Due to the high occupancy of 3d orbits, the introduction of Ni^{2+}, Cu^{2+}, or Zn^{2+} into the A_{Td}^{2+} of Co_3O_4 can couple the interactions of electron-repelling and π-donating in A_{Td}^{2+}-O-Co_{Oh}^{3+} [37]. As a result, the electronic structure of Co_{Oh}^{3+} is regulated to weaken the binding energy with Cl•, which can efficiently overflow from Co_{Oh}^{3+} sites for ammonia nitrogen oxidation. Besides, the binding energy and the matching degree of energy level between different A_{Td}^{2+} and NH_4^+ are elaborately analyzed. Through batch experiments and electrochemical characterizations, the mass transfer of NH_4^+ and production of Cl• in the systems with different anodes are compared and their effects on ammonia nitrogen oxidation are investigated. Combined with theoretical calculations, the enhanced removal mechanism of ammonia nitrogen is discerned. This study opens a new avenue for the efficient mineralization treatment of actual ammonia-nitrogen wastewater and guides the design and synthesis of superior anodes for environmental remediation.

The energy level differences (ΔE) of HOMO/LUMO and the binding energy between NH_4^+ and $Ni_{Td}^{2+}/Cu_{Td}^{2+}/Zn_{Td}^{2+}$ are systematically investigated. As illustrated in Fig. 1b, ΔE between NH_4^+ and $Cu_{Td}^{2+}/Zn_{Td}^{2+}$ is 1.66 and 1.19 eV, respectively, which is much lower than that of Ni_{Td}^{2+} (3.45 eV). A nearer energy level of HOMO/LUMO in two molecules is more conducive to forming more stable bonding orbitals [38–40]. Besides, the adsorption energy (E_{ads}) between the A_{Td}^{2+} sites of $A_xCo_{3-x}O_4$ (A_{Td}^{2+}: Ni_{Td}^{2+}, Cu_{Td}^{2+}, or Zn_{Td}^{2+}) and NH_4^+ is further analyzed. As shown in Fig. 1c and Fig. S1 (Supporting information), the value of E_{ads} between NH_4^+ and $Zn_xCo_{3-x}O_4$ is calculated to be merely −4.75 eV. Though a more stable bonding orbital between Zn_{Td}^{2+} and NH_4^+, Zn_{Td}^{2+} is relatively inert and cannot effectively enrich NH_4^+ because the 3d orbital of Zn^{2+} is fully filled by electrons ($3d^{10}$) (Fig. S2 in Supporting information). By contrast, Cu_{Td}^{2+} has higher binding energy (−6.83 eV) with NH_4^+ than Zn_{Td}^{2+} and Ni_{Td}^{2+} (−5.4 eV), which exhibits remarkable potential for enrichment of NH_4^+. $A_xCo_{3-x}O_4$ with spinel structure was successfully synthesized by the one-pot hydrothermal method and it is verified that the tetrahedral sites in Co_3O_4 are substituted by Ni_{Td}^{2+}, Cu_{Td}^{2+}, or Zn_{Td}^{2+} (Figs. 1d-f, Figs. S3-S12, Table S1 in Supporting information). Moreover, the mass transfer direction of NH_4^+ in the EC system was discerned over $A_xCo_{3-x}O_4$ anode. As shown in Fig. S13 (Supporting information), all anodes show no obvious adsorption performance for NH_4^+ under no current applied condition. In the absence of an electric field, NH_4^+ is uniformly distributed in the EC system and there is no concentration gradient between the anode and cathode regions. After the input of current (25 mA), the concentration of NH_4^+ in the Pt cathode region decreases significantly from 5 mmol/L to approximately 3.2 mmol/L within 20 min, while that of the $Cu_xCo_{3-x}O_4$ anode region exhibits slow decreasing trends (4.3 mmol/L, 20 min). A distinct concentration gradient of NH_4^+ is observed between the $Cu_xCo_{3-x}O_4$ anode and cathode regions, which is more significant than that in the EC system with $Ni_xCo_{3-x}O_4$, $Zn_xCo_{3-x}O_4$ or Co_3O_4 anode (Figs. S14-S16 in Supporting information). Due to the strong interaction between Cu_{Td}^{2+} and NH_4^+, the dynamic mass transfer of NH_4^+ from the cathode region to the anode region and from the solution to the anode interface occurs, resulting in the concentration of NH_4^+ in the anode region much higher than that in the cathode region. This phenomenon demonstrates that $Cu_xCo_{3-x}O_4$ can overcome the electrostatic repulsion between NH_4^+ and anode, which is conducive to effective reaction with active species at the anodic interface.

To further visualize the enrichment of NH_4^+ at the anode interface, X-ray photoelectron spectroscopy (XPS) and *in-situ* Raman spectra were carried out. No obvious characteristic peak of NH_4^+ is observed in the N 1s XPS of the $Ni_xCo_{3-x}O_4$, $Zn_xCo_{3-x}O_4$ and Co_3O_4 anodes before and after the input of current (Figs. S17-S19 in Supporting information). As a comparison, when $Cu_xCo_{3-x}O_4$ is the anode, the characteristic peak of N–H bond in NH_4^+ emerges after the input of current, indicating NH_4^+ can efficiently enrich at the $Cu_xCo_{3-x}O_4$ anode (Fig. S20 in Supporting information). *In-situ* Raman spectra provide more evidence that the introduction of Cu_{Td}^{2+} enhances the mass transfer of NH_4^+ to the anode. As shown in Fig. 1h, the peaks around 1590 cm^{-1} *in-situ* Raman spectra of the $Cu_xCo_{3-x}O_4$ system are assigned to the antisymmetric bending vibration of the HNH of NH_3 [41–43]. The intensity of these peaks first increases and then decreases during the reaction, indicating that NH_4^+ can overcome the electrostatic interactions to enrich and be further oxidized on Cu_{Td}^{2+}. The intensity of the A_{1g} peak first decreases and then increases during the reaction, which is attributed to the cycling of Co^{3+}/Co^{2+} at the octahedral sites for the activation of Cl^-. The negligible peaks around 1590 cm^{-1} in the *in-situ* Raman spectra of the $Ni_xCo_{3-x}O_4$, $Zn_xCo_{3-x}O_4$, and Co_3O_4 anodes illustrate the interactions between NH_4^+ and the $Ni_xCo_{3-x}O_4/Zn_xCo_{3-x}O_4/Co_3O_4$ anodes are weak, leading to the in-

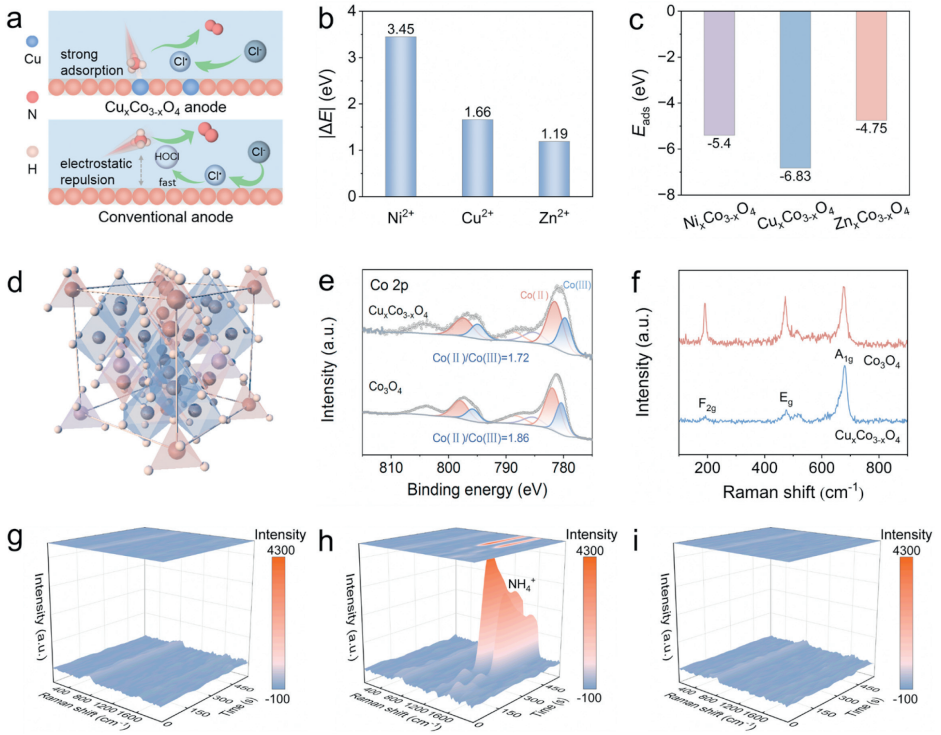


Fig. 1. (a) Schematic mechanism of enhanced ammonia oxidation by $Cu_xCo_{3-x}O_4$ compared to conventional anode. (b) DFT-calculated LUMO and HOMO energy level differences between A^{2+} and NH_4^+ (A^{2+}: Ni^{2+}, Cu^{2+}, Zn^{2+}). (c) Adsorption energy between NH_4^+ and the A_{Td}^{2+} site in $A_xCo_{3-x}O_4$ electrodes. (d) Crystal structure of $Cu_xCo_{3-x}O_4$. (e) XPS spectra for Co 2p and (f) Raman spectroscopy of Co_3O_4 before and after modification with Cu. *In-situ* Raman spectroscopy of (g) $Ni_xCo_{3-x}O_4$, (h) $Cu_xCo_{3-x}O_4$, and (i) $Zn_xCo_{3-x}O_4$.

ability of transferring NH_4^+ to the anode under electrostatic repulsion (Figs. 1g and i and Fig. S21 in Supporting information). Based on the above results, it is confirmed that $Cu_xCo_{3-x}O_4$ can efficiently induce NH_4^+ to overcome the electrostatic repulsion and realize its enrichment at the anode due to the strong interaction and moderate energy level matching between Cu_{Td}^{2+} and NH_4^+, which facilitates rapid reaction with interfacial active species and thus efficient mineralization.

The removal performance of ammonia-nitrogen was investigated in the EC system with different anodes. As shown in Fig. 2a and Fig. S22 (Supporting information), 100 % of NH_4^+-N is removed in the EC system with $Cu_xCo_{3-x}O_4$ anode within 80 min at a k_{obs} of 4.4×10^{-2} min^{-1}, which is more remarkable than Co_3O_4 (2.2×10^{-2} min^{-1}) and commercial dimensionally stable anode (DSA) (0.7×10^{-2} min^{-1}). It is worth noting that the introduction of Fe_{Td}^{2+}, Mn_{Td}^{2+}, Ni_{Td}^{2+}, and Zn_{Td}^{2+} into the Co_3O_4 anode does not significantly improve the NH_4^+-N removal performance. Since there is no special interaction between NH_4^+ and $A_xCo_{3-x}O_4$ (A = Fe, Mn, Ni, Zn) anode, NH_4^+ cannot enrich at the anode limited by electrostatic repulsion, resulting in that NH_4^+-N cannot react in time with the anodic interface Cl•. As a comparison, the $Cu_xCo_{3-x}O_4$ anode can efficiently enrich NH_4^+ and achieve efficient mineralization of ammonia nitrogen by interfacial Cl•. Besides, as demonstrated in Figs. 2b and c, the concentration of TN decreases simultaneously with the reduction of ammonia concentration and no undesirable products (such as NO_2^-, NO_3^-) are generated after the reaction. Although a small amount of chloramines (NH_2Cl, $NHCl_2$, and NCl_3) are produced during the reaction process, they are completely converted into N_2 as the reaction progresses. Moreover, five cycle experiments were performed to evaluate the durability of $Cu_xCo_{3-x}O_4$ electrodes. As shown in Fig. S23 (Supporting information), the degradation of NH_4^+-N remains essentially unchanged after five consecutive runs. The morphology, structure and Co^{2+}/Co^{3+} ratio of the $Cu_xCo_{3-x}O_4$ anode after five cycles are basically consistent with that before the reaction, and the leaching concentrations of cobalt ions are <0.6 mg/L and those of copper ions are <0.3 mg/L after each cycle (Figs. S24-S28 in Supporting information). These results confirm that the $Cu_xCo_{3-x}O_4$ anode has excellent stability. In addition, to further explore the feasibility of the practical application of the $Cu_xCo_{3-x}O_4$ anode, the cost analysis for ammonia nitrogen degradation is performed. As exhibited in Fig. 2d, Tables S2 and S3 (Supporting information), no matter the electrode cost or energy consumption, the $Cu_xCo_{3-x}O_4$ anode (0.44 $/piece, 15.1 kWh/$kg_{-N}$) is superior to DSA (1.47 $/piece, 31.3 kWh/$kg_{-N}$) and other ammonia oxidation reaction (AOR) anodes reported by the previous literature.

To confirm the feasibility of $Cu_xCo_{3-x}O_4$ anode for the treatment of practical ammonia-nitrogen wastewater (pH 7.51), further experiments are constructed to evaluate its high activity. The main components of landfill leachate are presented in Table S4 (Supporting information) and the NH_4^+-N concentration in the raw wastewater is 332.6 mg/L. As shown in Fig. 2e, the EC system assembled with $Cu_xCo_{3-x}O_4$ anode exhibits a significantly higher NH_4^+-N removal and mineralization performance (99.1 %, 70.7 %) within 8 h than that with Co_3O_4 anode (85.9 %, 60.1 %) and DSA (55.8 %, 40.0 %) (Fig. 2f and Fig. S29 in Supporting information). More importantly, the scale-up experiment in a flow electrolyzer with $Cu_xCo_{3-x}O_4$ anode realizes 100 % of NH_4^+-N and 88.3 % of total nitrogen (TN) removal during the four days continuous operation without an obvious decline in catalytic performance (Figs. 2g-i), which is also much superior to the system with DSA (NH_4^+-N: 77.2 %, TN: 66.1 %) (Figs. S30 and S31 in Supporting information). Besides, the peak shapes and positions of the XRD diffraction peaks and Raman peaks of the $Cu_xCo_{3-x}O_4$ electrodes remained almost unchanged after the long-term reaction, indicating that the $Cu_xCo_{3-x}O_4$ electrodes have good stability (Figs. S32 and S33 in Supporting information). In conclu-

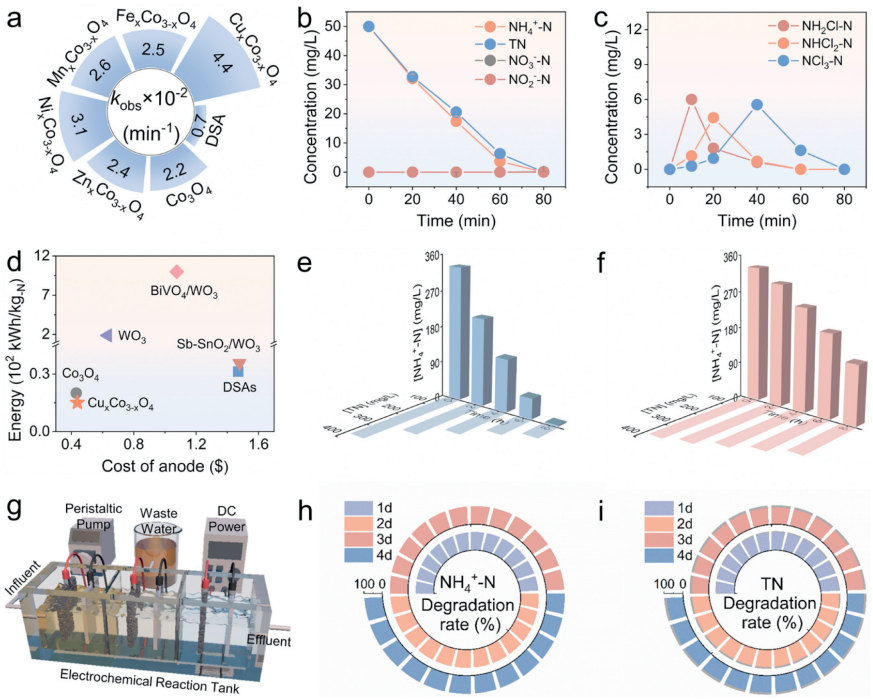


Fig. 2. (a) Ammonia nitrogen removal performance in the EC system using different anodes. Concentrations of (b) different nitrogen species and (c) chloramine in the EC system with $Cu_xCo_{3-x}O_4$ anode. (d) Cost analysis of different systems for ammonia removal. Ammonia and total nitrogen removal performance of (e) $Cu_xCo_{3-x}O_4$ and (f) DSA anodes for treatment of practical wastewater. (g) Diagram showing the electrochemical reaction tank with multipairs of electrodes for landfill leachate treatment under continuous flow conditions. Time-dependent degradation rate of (h) NH_4^+-N and (i) total nitrogen for continuous treatment of landfill leachate by the $Cu_xCo_{3-x}O_4$ system with 3 pairs of electrodes.

sion, $Cu_xCo_{3-x}O_4$ demonstrates extraordinary activity for NH_4^+-N mineralization and excellent feasibility for the purification of practical ammonia-nitrogen wastewater.

Electron paramagnetic resonance (EPR) technology and quenching experiments were performed to verify the active species during the NH_4^+ mineralization process. An EPR signal with eleven-lines is observed in the EC system with Co_3O_4 and $Cu_xCo_{3-x}O_4$ anodes during the electrolysis of NaCl solution (Fig. 3a), corresponding to DMPO–OH$^\bullet$ and DMPO–Cl$^\bullet$ [44]. Compared with the Co_3O_4 anode, the higher signal intensity of DMPO–Cl$^\bullet$ on the $Cu_xCo_{3-x}O_4$ anode indicates the introduction of Cu_{Td}^{2+} facilitates the production of Cl$^\bullet$. After the addition of NH_4^+-N to the EC system with $Cu_xCo_{3-x}O_4$ anode, the DMPO–Cl$^\bullet$ signal disappears and the DMPO–OH$^\bullet$ signal is retained, confirming that NH_4^+-N is susceptible to oxidation by Cl$^\bullet$ relative to OH$^\bullet$ (Fig. 3b). The role of Cl$^\bullet$ was further investigated using different quenchers. Hyposulphite ($Na_2S_2O_3$) is the quencher for OH$^\bullet$, Cl$^\bullet$ and free chlorines; tertiary butanol (TBA) for OH$^\bullet$, Cl$^\bullet$ and ClO$^\bullet$; bicarbonate (HCO_3^-) for OH$^\bullet$, Cl$^\bullet$ and $Cl_2^{\bullet-}$; *p*-chlorobenzoic acid (PCBA) for OH$^\bullet$ (Table S5 in Supporting information) [45]. As shown in Figs. S34 and S35 (Supporting information), NH_4^+-N is barely degraded using $Na_2S_2O_3$ as a quencher, confirming that direct oxidation of NH_4^+-N on the $Cu_xCo_{3-x}O_4$ anode is difficult. PCBA shows a slight inhibitory effect on ammonia degradation, suggesting a limited role for OH$^\bullet$. The degradation of NH_4^+-N is significantly inhibited by the addition of HCO_3^- (49.2 %, 80 min), suggesting that both Cl$^\bullet$ and $Cl_2^{\bullet-}$ are involved. According to previous studies, NH_4^+-N has much higher reaction rates with Cl$^\bullet$ than $Cl_2^{\bullet-}$ (Table S6 in Supporting information), indicating Cl$^\bullet$ mediated radical oxidation plays a major role in NH_4^+-N oxidation. The contribution of different active species to ammonia oxidation is evaluated and quantified based on the specific subtraction of ammonia oxidation rate constants for different quenchers (Fig. 3c). The detailed calculation of the contribution of each active species is shown in Fig. S36 (Supporting information). The Cl$^\bullet$ is mainly responsible (about 74.6 %) for the overall ammonia oxidation. In addition, the concentration variation and current efficiency (η) of free chlorines (Cl_2, ClO^-, and HClO) in the different systems is quantified (Fig. S37 in Supporting information). Compared to DSA and Co_3O_4, The $Cu_xCo_{3-x}O_4$ system exhibits enhanced free chlorine production and higher current efficiency, further demonstrating that the introduction of Cu_{Td}^{2+} facilitates Cl$^\bullet$ generation.

The Cl$^\bullet$ generation and ammonia oxidation activities of the $Cu_xCo_{3-x}O_4$ anode are investigated by varied electrochemical characterizations. As shown in Fig. 3d, a higher current density is observed in the linear sweep voltammetry (LSV) curve with $Cu_xCo_{3-x}O_4$ anode than that with Co_3O_4 anode, and the current density is significantly increased after adding NH_4^+. Although the introduction of Cu_{Td}^{2+} of Co_3O_4 does not significantly increase CER performance, the AOR activity is greatly promoted because NH_4^+-N can efficiently react with the interfacial Cl$^\bullet$. Besides, the Tafel slopes of the $Cu_xCo_{3-x}O_4$ anode are markedly lower than that of the Co_3O_4 anode in the absence and presence of NH_4^+ (Fig. 3e), indicating that the $Cu_xCo_{3-x}O_4$ anode exhibits superior kinetics for Cl$^\bullet$ generation and AOR. Moreover, a redox peak is observed in the cyclic voltammogram (CV) curve around 1.5 V for both Co_3O_4 and $Cu_xCo_{3-x}O_4$ anodes (Fig. 3f), attributing to Co^{2+}/Co^{3+}. Specifically, only one anodic peak appeared at 1.65 V for the $Cu_xCo_{3-x}O_4$ anode, indicating that Cu_{Td}^{2+} can promote the cycle of Co^{2+}/Co^{3+} to achieve efficient Cl$^\bullet$ generation. In addition, the electrochemical surface area (ECSA) of the electrodes is explored by the electrochemical double-layer capacitance (C_{dl}) to compare their intrinsic activities. Figs. S38 and S39 (Supporting information) illustrate that the C_{dl} value and intrinsic activity of the $Cu_xCo_{3-x}O_4$ anode are significantly higher than that of the Co_3O_4 anode, providing further evidence that the introduction of Cu^{2+} into the $Cu_xCo_{3-x}O_4$ increases the active sites for Cl$^\bullet$ production.

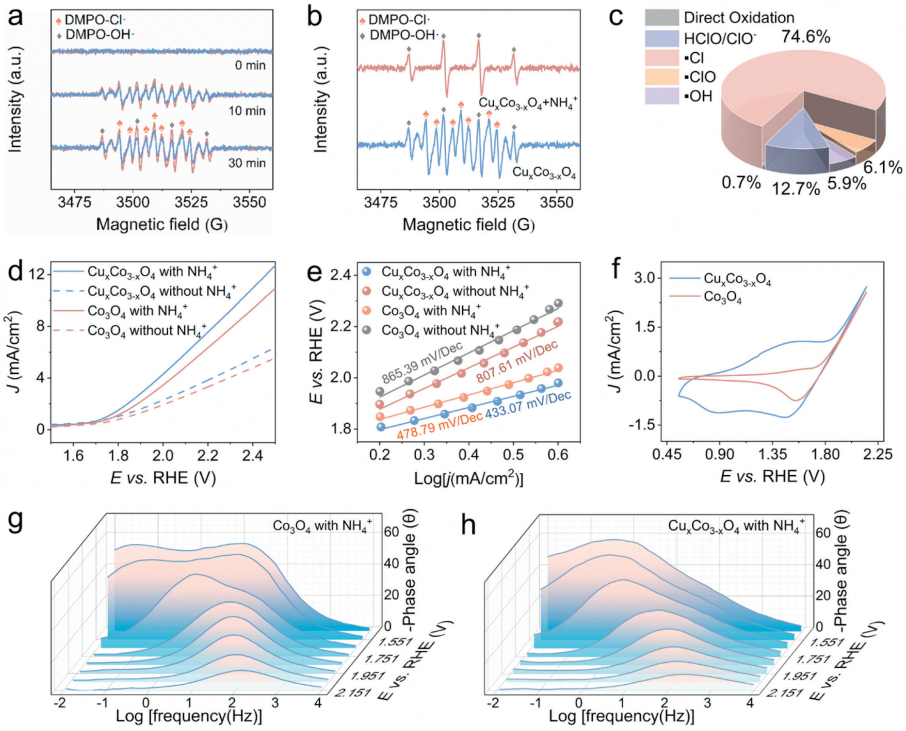


Fig. 3. (a) EPR spectra in $Cu_xCo_{3-x}O_4$/NaCl (brown line) and Co_3O_4/NaCl (blue line) systems. Conditions: [NaCl] = 60 mmol/L, constant current = 25 mA. (b) EPR spectra. Conditions: [NaCl] = 60 mmol/L, constant current = 25 mA. (c) Contributions of different active species in the $Cu_xCo_{3-x}O_4$ system. (d) LSV curves of $Cu_xCo_{3-x}O_4$ and Co_3O_4. Condition: [NaCl] = 60 mmol/L, scan rate: 5 mV/s. (e) Tafel slopes of $Cu_xCo_{3-x}O_4$ and Co_3O_4 anodes. Conditions: [NaCl] = 60 mmol/L. (f) Cyclic voltammetry (CV) of Co_3O_4 and $Cu_xCo_{3-x}O_4$ anodes. Conditions: [NaCl] = 60 mmol/L, scan rate: 5 mV/s. Bode phase diagrams of the operando EIS measurements on (g) Co_3O_4 and (h) $Cu_xCo_{3-x}O_4$ in the presence of NH_4^+.

Electrocatalytic reaction kinetics and electrode/electrolyte interface properties are further investigated through electrochemical impedance spectroscopy (EIS). As shown in Figs. S40 and S41 (Supporting information), a transition peak at the 1.65 V potential is observed for both Co_3O_4 and $Cu_xCo_{3-x}O_4$ anodes. The transition peak is related to the unevenness charge contribution caused by the formation of oxidizing species on the electrode surface [46]. The transition peaks shift to higher frequencies and lower phase angles as the potential rises in CER processes. The frequency and phase angle of the $Cu_xCo_{3-x}O_4$ anode varies to a greater extent relative to Co_3O_4 with the increase of bias voltage, which indicates that the introduction of Cu_{Td}^{2+} enhances the Cl• generation activity. Notably, an earlier and lower-frequency transition peak at the potential of 1.55 V is observed for the $Cu_xCo_{3-x}O_4$ anode after the addition of NH_4^+ (Figs. 3g and h). These results indicate that the introduction of Cu^{2+} into the tetrahedral site of Co_3O_4 can effectively enrich NH_4^+ and enhance the NH_4^+-N oxidation performance.

By comparing the electronic structure of Co_{Oh}^{3+} sites and the adsorption capacity of reaction intermediates before and after Cu doping, the enhanced removal mechanism of ammonia nitrogen over the $Cu_xCo_{3-x}O_4$ anode is elaborately studied. As shown in Figs. 4a and b, the shift of the Co 2p XPS to the higher binding energies emerges after the introduction of Cu_{Td}^{2+} into Co_3O_4, indicating an increase in electron cloud density around Co(II)/Co(III) in $Cu_xCo_{3-x}O_4$ compared to Co_3O_4. Besides, the differential charge density and Bader charge of the different anodes are further conducted. As illustrated in Fig. 4c, the district around Cu_{Td}^{2+} is predominantly electronic dissipating (green), while the district around Co_{Oh}^{3+} is predominantly electronic accumulating (purple), indicating that electrons around Cu_{Td}^{2+} migrate towards Co_{Oh}^{3+}. The Bader charge analysis shows that the introduction of Cu_{Td}^{2+} modulates the charge of the adjacent Co_{Oh}^{3+} from 1.22 to 1.24. As a result, the adsorption energy of Cl^- at the Co_{Oh}^{3+} sites is weakened from −0.15 eV to −0.10 eV (Fig. 4d), which could facilitate Cl• overflowing from Co_{Oh}^{3+} for NH_4^+-N oxidation. Finally, the Gibbs free energy of the Cl• generation process is calculated by DFT to further understand the effect of Cu doping. During the Cl• generation process, the rate-determining step (RDS) is the desorption of Cl* from Co_{Oh}^{3+}, and its energy barrier is reduced from 2.57 eV to 2.52 eV by Cu doping (Fig. 4e). The results indicate that Cu doping facilitates the desorption of Cl* from Co_{Oh}^{3+} sites, thereby promoting the Cl• for NH_4^+-N oxidation.

In conclusion, the enhanced removal mechanism of NH_4^+-N over the $Cu_xCo_{3-x}O_4$ anode is explained as follows. The introduction of Cu_{Td}^{2+} into Co_3O_4 induces the enrichment of NH_4^+ at the anode by utilizing the strong interaction between NH_4^+ and Cu^{2+}. Subsequently, the tetrahedral substitution of Cu^{2+} in Co_3O_4 can modulate the electronic structure of the Co_{Oh}^{3+} and promote the overflow of Cl• from Co_{Oh}^{3+}, thus achieving the efficient and selective mineralization of NH_4^+-N by interfacial Cl•.

In this study, we introduce Cu_{Td}^{2+} into the tetrahedral sites of Co_3O_4 to enhance the mass transfer of NH_4^+ and weaken the binding energy of Cl• at the Co_{Oh}^{3+} sites for the selective and efficient NH_4^+-N mineralization induced by interfacial Cl•. Compared to Ni_{Td}^{2+} and Zn_{Td}^{2+}, Cu_{Td}^{2+} has moderate energy level matching and strong binding energy with NH_4^+, which results in NH_4^+ effectively overcoming electrostatic repulsion and enriching at the anode. Meanwhile, the electronic interactions of Cu_{Td}^{2+}-O-Co_{Oh}^{3+} bonds increase the electron cloud density, weakening the binding energy of Cl• at the Co_{Oh}^{3+} sites, which is conducive to the separation of Cl• from the interface, and then reacting with NH_4^+-N. As a result, NH_4^+-N is efficiently mineralized into N_2 with low cost and energy consumption in the EC system assembled with $Cu_xCo_{3-x}O_4$ anode, superior to which is much that of the commercial DSA. Notably, the system exhibits excellent activity and durability in treat-

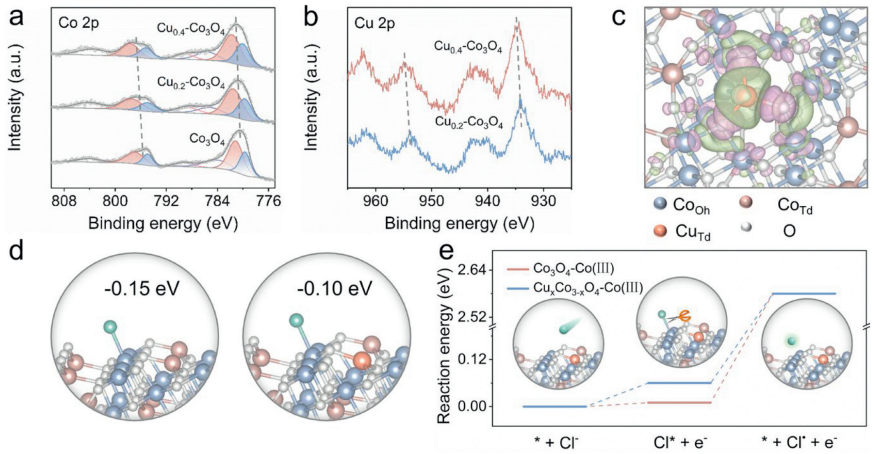


Fig. 4. XPS spectra of (a) Co 2p and (b) Cu 2p orbitals of Co_3O_4 with different Cu introductions. (c) Differential charge density diagram of $Cu_xCo_{3-x}O_4$. (d) Adsorption energy between Cl^- and the structural Co(III) in Co_3O_4 and $Cu_xCo_{3-x}O_4$ electrodes. (e) Gibbs energy diagrams for the $Cl^•$ generation reaction on Co_3O_4-Co(III) and $Cu_xCo_{3-x}O_4$-Co(III).

ing high concentrations of NH_4^+-N from practical landfill leachate under continuous flow operation, confirming its excellent application potential. This paper provides a new idea for the efficient mineralization treatment of actual ammonia-nitrogen wastewater.

Declaration of competing interest

The authors declare that they have no known competing financial interests or personal relationships that could have appeared to influence the work reported in this paper.

CRediT authorship contribution statement

Xia Chen: Writing – original draft, Software, Investigation, Formal analysis, Data curation. **Ting Dai:** Investigation. **Meng-Ying Yin:** Formal analysis. **Xing-Yuan Xia:** Software. **Qiu-Ju Xing:** Visualization, Supervision. **Lei Tian:** Writing – review & editing, Writing – original draft, Supervision, Methodology, Conceptualization. **Jian-Ping Zou:** Writing – review & editing, Project administration, Funding acquisition, Conceptualization.

Acknowledgments

This work was supported by the National Natural Science Foundation of China (Nos. 52300081, 52170082, 52470079, 51938007, and 52100186), the Postdoctoral Fellowship Program of China Postdoctoral Science Foudation (CPSF) (No. GZB20240175), the China Postdoctoral Science Foundation (No. 2024M750620), the Natural Science Foundation of Jiangxi Province (No. 20212ACB203008), and Key Laboratory of Jiangxi Province for Persistent Pollutants Prevention Control and Resource Reuse (No. 2023SSY02061). We are grateful for the financial support of the projects and research platform support provided by the laboratory.

Supplementary materials

Supplementary material associated with this article can be found, in the online version, at doi:10.1016/j.cclet.2025.111445.

References

[1] O. Deng, S. Wang, J. Ran, et al., Nat. Commun. 15 (2024) 401.
[2] M.R. Adam, M.H.D. Othman, R.A. Samah, et al., Sep. Purif. Technol. 213 (2019) 114–132.
[3] A. Lintern, L. McPhillips, B. Winfrey, J. Duncan, C. Grady, Environ. Sci. Technol. 54 (2020) 9159–9174.
[4] R. Ma, K. Li, Y. Guo, et al., Nat. Commun. 12 (2021) 6308.
[5] O. Deng, S. Huang, C. Wang, et al., Environ. Sci. Technol. 58 (2024) 449–458.
[6] H.Y. Liu, J.A. Jayworth, R.H. Crabtree, G.W. Brudvig, ACS Catal. 14 (2024) 2842–2846.
[7] G. Mutahi, J.B. van Lier, H. Spanjers, Water Res. 265 (2024) 122296.
[8] C. Shin, A. Szczuka, M.J. Liu, et al., Environ. Sci. Technol. 56 (2022) 8712–8721.
[9] Z. Hu, T. Liu, Z. Wang, J. Meng, M. Zheng, Environ. Sci. Technol. 57 (2023) 4522–4532.
[10] J.J. Wang, B.C. Huang, J. Li, R.C. Jin, Chin. Chem. Lett. 31 (2020) 2567–2574.
[11] Y.H. Chuang, T.Y. Chen, C.S. Chou, et al., Environ. Sci. Technol. 57 (2023) 15232–15242.
[12] Y. Liu, Y. Zhu, W. Duan, et al., Chin. Chem. Lett. 36 (2025) 110347.
[13] C. Zhang, D. He, J. Ma, T.D. Waite, Water Res. 145 (2018) 220–230.
[14] X. Huang, Y. Zhang, J. Bai, et al., Chem. Eng. J. 392 (2020) 123695.
[15] Y. Chen, G. Zhang, Q. Ji, et al., Environ. Sci. Technol. 56 (2022) 9722–9731.
[16] L. Tian, X.Y. Xia, L.J. Zhou, et al., Appl. Catal. B: Environ. Energy 340 (2024) 123260.
[17] Y. Chen, X. Xia, L. Tian, et al., Chin. Chem. Lett. 35 (2024) 109789.
[18] P. Jiang, T. Zhou, J. Bai, et al., Water Res. 235 (2023) 119914.
[19] Y. Zhou, H. Wang, X. Liu, et al., Appl. Catal. B: Environ. Energy 294 (2021) 120265.
[20] D. Minakata, D. Kamath, S. Maetzold, Environ. Sci. Technol. 51 (2017) 6918–6926.
[21] Y. Lei, X. Lei, P. Westerhoff, X. Zhang, X. Yang, Environ. Sci. Technol. 55 (2021) 689–699.
[22] Y. Zhang, J. Li, J. Bai, et al., Environ. Sci. Technol. 52 (2018) 1413–1420.
[23] C. Zhou, J. Li, J. Wang, et al., Appl. Catal. B: Environ. Energy 324 (2023) 122229.
[24] J. Sun, L. Liu, F. Yang, Appl. Catal. B: Environ. Energy 308 (2022) 121215.
[25] N. Chen, J. Ruan, S. Lu, Z. Sun, G. Zhang, ACS ES&T Water 2 (2022) 1132–1142.
[26] H. Ha, K. Jin, S. Park, et al., J. Phys. Chem. Lett. 10 (2019) 1226–1233.
[27] S. Zhao, H. Li, J. Dai, et al., Nat. Sustain. 7 (2024) 148–157.
[28] X. Zhang, D. Wu, X. Liu, et al., Appl. Catal. B: Environ. Energy 330 (2023) 122594.
[29] S. Xing, N. Liu, Q. Li, et al., Nat. Commun. 15 (2024) 4951.
[30] J. Wang, L. Zhao, Y. Zou, et al., J. Am. Chem. Soc. 146 (2024) 11152–11163.
[31] F. Zhang, Z. Du, J. Wang, Y. Du, Y. Peng, Water Res. 260 (2024) 121921.
[32] Z. Wang, J. Huang, L. Wang, et al., Angew. Chem. Int. Ed. 61 (2022) e202114696.
[33] H. Luo, J. Deng, Q. Gou, et al., Chin. Chem. Lett. 34 (2023) 107885.
[34] Q. Hu, S. Qi, Q. Huo, et al., J. Am. Chem. Soc. 146 (2024) 2967–2976.
[35] Y. Zhang, X. Huang, J. Li, et al., Environ. Sci. Technol. 56 (2022) 9693–9701.
[36] W. Hu, M. Zheng, H. Duan, et al., Chin. Chem. Lett. 33 (2022) 1412–1416.
[37] L. Tian, Z.J. Tang, L.Y. Hao, et al., Angew. Chem. Int. Ed. 63 (2024) e202401434.
[38] J. Luo, L. Xu, Y. Zhou, et al., Angew. Chem. Int. Ed. 62 (2023) e202302302.
[39] Z.Q. Xu, R. Zou, W.W. Liu, et al., Chem. Eng. J. 471 (2023) 144581.
[40] Z.Z. Dong, J.H. Zhang, L. Zhu, et al., Chin. Chem. Lett. 36 (2025) 109773.
[41] W. Gao, K. Xie, J. Xie, et al., Adv. Mater. 35 (2023) 2202952.
[42] L. Bai, F. Franco, J. Timoshenko, et al., J. Am. Chem. Soc. 146 (2024) 9665–9678.
[43] J.Y. Fang, Q.Z. Zheng, Y.Y. Lou, et al., Nat. Commun. 13 (2022) 7899.
[44] Y. Zhang, J. Li, J. Bai, et al., Appl. Catal. B: Environ. Energy 238 (2018) 168–176.
[45] W. Kuang, Z. Yan, J. Chen, et al., Environ. Sci. Technol. 57 (2023) 18538–18549.
[46] L. Cai, Y. Liu, J. Zhang, et al., J. Energy Chem. 92 (2024) 95–103.